

# On The Diffusion of Sticky Particles in 1-D

Joshua DM Hellier\* and Graeme J Ackland†  
SUPA, School of Physics and Astronomy, University of Edinburgh,  
Mayfield Road, Edinburgh EH9 3JZ, United Kingdom  
(Dated: January 5, 2018)

This is where I would write the abstract. This is probably best left until the end, as then I'll know what I'm actually summarising.

## I. INTRODUCTION

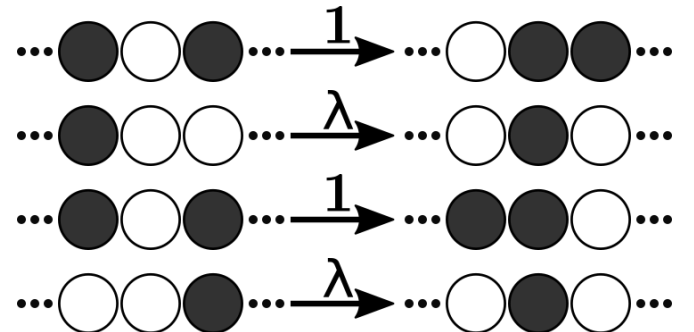
Lattice gases are a ubiquitous tool for modelling complex systems from biology to traffic[1, 2]. One example is the oxidation process, as occurs in the growth of an oxide layer on a metallic surface. Almost all uncoated metallic objects [Al, Ti, Ca, Zr, Sn] are protected by such a thin, self-assembling layer, driven by the oxidation potential but arrested by the slow kinetics of transporting material through the oxide layer [3–6].

Analytically solvable cases involve non-interacting or excluding particles [7, 8]. But in any real system of interest the moving objects interact. Many models tackle the situation where the diffusing object interact with the substrate, but despite the clear application-relevance there is surprisingly little work considering interactions between the moving particles. One reason for this is that the interactions introduce nonlinearities in analytical models, which makes them challenging to solve. This is unfortunate, because it is precisely these nonlinearities which introduce interesting behaviours - discontinuities at the oxide-metal interface, diffusion instability, to name just a few. In this paper we will introduce (or perhaps more properly, revive) a simple 1-dimensional model, specified in Figure 1, which contains such an interaction, and we will explore the impact this has, particularly on behaviour in the large-scale limit. One might compare and contrast this approach (making a simple microscopic model and trying to learn about large-scale interface growth from it) with approaches such as the KPZ equation [9, 10].

### A. Model Definition

Our model, which we will refer to as the “Sticky Particle Model” or SPM, is essentially the same as the symmetric exclusion process [11], the difference being that adjacent particles separate with rate  $\lambda = 1 - \zeta$  instead of their normal hopping rate, 1. It is in fact a rephrasing of the KLS model [12, 13] in 1-dimension without an applied field, which is itself similar to the dynamics used to analyse the Ising model by Kawasaki [14]. It seems that

FIG. 1. White circles indicate particles, dark circles indicate empty sites (vacancies). Particles randomly move into adjacent vacancies with rate 1 (having rescaled time for notational convenience), unless there is a particle behind the position they're moving from, in which case they move with rate  $\lambda = 1 - \zeta$ .



this symmetric model has not been researched much, at least in terms of its dynamics, because the model with the applied field is so interesting; however, it seems that the simple symmetric model is also capable of doing interesting things under an applied concentration gradient.

We have chosen to specify things primarily in terms of  $\zeta$  instead of  $\lambda$  because it makes many of the analytic results much neater, whilst intuitively representing “stickiness”, as particles tend to clump when  $\zeta > 0$  and separate when  $\zeta < 0$ . It is worth noting that the rates specified in Figure 1 obey detailed balance, with an energy proportional to the number of particle-particle adjacencies in the system. One can show that there exists an isomorphism between this model and the Misanthrope Process [15]. This doesn't help us to solve the model in the kinds of steady flow cases we are mainly interested in due to difficulties with the boundary conditions, but it does allow us to show that this model does **not** exhibit explosive condensation [16].

## II. MODEL PHENOMENOLOGY

The model described in Figure 1 is very simple, but numerical simulation shows that it is capable of a wide range of behaviours, such as those shown in Figure 5. We will discuss these numerical results in more detail in Section III, but first let us try to predict the model behaviour using analytic means.

\* J.D.M.Hellier@sms.ed.ac.uk

† G.J.Ackland@ed.ac.uk

### A. Mean-Field Theory Derivation

Let the spacing between lattice sites be  $a$ ,  $\tau_0$  be the non-sticky hopping timescale and the time-averaged (or ensemble-averaged, assuming ergodicity) occupation probability of the  $i^{\text{th}}$  lattice site be  $\rho_i$ . One may show that, in the mean-field approximation regime,

$$\begin{aligned} \tau_0 \frac{\partial \rho_i}{\partial t} &= (1 - \rho_i) [(1 - \zeta \rho_{i-2}) \rho_{i-1} + (1 - \zeta \rho_{i+2}) \rho_{i+1}] \\ &\quad - \rho_i [2\zeta \rho_{i-1} \rho_{i+1} - (3 - \zeta) (\rho_{i-1} + \rho_{i+1}) + 2], \end{aligned}$$

Switching to the continuum limit by taking  $a \rightarrow 0$ , and neglecting  $\mathcal{O}(a^4)$  terms, we may reexpress this as a conserved flow  $J$  as follows:

$$\begin{aligned} \frac{\partial \rho}{\partial t} &= -\frac{\partial J}{\partial x}, \\ J &= -\frac{a^2}{\tau_0} A(\rho) \frac{\partial \rho}{\partial x}, \\ A &= 1 - \zeta \rho(4 - 3\rho). \end{aligned}$$

Thus, the MFT says that the particles should diffuse with a diffusion coefficient which depends upon the local density.

### B. Continuum MFT Predictions

First let us consider some limits. As  $\zeta \rightarrow 0$  (in other words, as the model becomes a simple exclusion model),  $A \rightarrow 1$ , which makes sense. Likewise, in the dilute limit  $\rho \rightarrow 0$ ,  $A \rightarrow 1$ , reflecting the fact that it becomes a dilute lattice gas and therefore the interactions between particles become irrelevant as they never meet. Conversely, in the full limit  $\rho \rightarrow 1$ ,  $A \rightarrow 1 - \zeta$ ; this makes sense because we now have a dilute gas of vacancies, which hop with rate  $\lambda = 1 - \zeta$ . One may observe that the continuum limit MFT has a symmetry under  $\rho \mapsto \frac{4}{3} - \rho$ ; thus, the dynamics should be symmetric under a density profile reflection around  $\rho = \frac{2}{3}$ . This is where  $A$  always attains its extremal value,  $1 - \frac{4}{3}\zeta$ , hence for  $\zeta > 3/4$  the diffusion coefficient becomes negative in regions with  $\frac{2}{3} - \frac{\sqrt{\zeta(4\zeta-3)}}{3\zeta} < \rho < \frac{2}{3} + \frac{\sqrt{\zeta(4\zeta-3)}}{3\zeta}$ . Finally, it is possible to show that solutions to the continuum MFT containing domains with a negative diffusion coefficient are linearly unstable; thus, if we try to have a flow containing  $\rho$  for which  $A(\rho) < 0$ , the density of the medium should gravitate towards a density for which  $A(\rho) \sim 0$ , so instead of observing “backwards diffusion” we would see an extremely slow flow or no flow at all. The MFT implies that the transition to this critically slowly-flowing regime happens suddenly, like a phase transition; this is something we can check with our numerics.

### C. Steady-State Flow Through a Block

It is possible to solve the continuum MFT in a steady state on a finite domain, say  $x \in (0, L)$ . The continuity equation implies that  $J(x) = J_0$ , and by integrating both sides of our current equation with respect to  $x$  we find that

$$J_0(x - x_0) = -\frac{a^2}{\tau_0} \rho [1 + \zeta \rho (\rho - 2)], \quad (1)$$

a cubic equation which can be solved to give  $\rho(x)$ . If we impose Dirichlet boundary conditions on this system, say  $\rho(0) = \rho_0$  and  $\rho(L) = \rho_L$ , we find that

$$J = \frac{a^2}{L\tau_0} [\rho_0 - \rho_L + \zeta (\rho_0 [\rho_0^2 - 2] - \rho_L [\rho_L^2 - 2])]. \quad (2)$$

We may consider applying small concentration gradients across a block by setting  $\rho_0 = \rho_M + \frac{1}{2}\delta\rho$  and  $\rho_L = \rho_M - \frac{1}{2}\delta\rho$ . Doing so, we find that the effective diffusion coefficient of the block  $D = \frac{\partial J}{\partial \delta\rho}|_{\delta\rho=0}$  obeys

$$\frac{\partial J}{\partial \delta\rho} \Big|_{\delta\rho=0} = \frac{a^2}{L\tau_0} [1 - \zeta \rho_M (4 - 3\rho_M)], \quad (3)$$

a result we will make use of when we come to analyse our numerics in Section III.

## III. NUMERICAL RESULTS

We now have some MFT predictions about the SPM, and a few ideas about when those predictions might be invalid. Thus, it is prudent for us to test them out numerically. There are a few different methods which could have been used, but we chose to calculate using the excellent **KMCLib**[17] package, which implements the Kinetic Monte Carlo algorithm (essentially the same as the Gillespie algorithm) on lattice systems. **KMCLib** has the advantage that it is python-wrapped C++, and thus quite easy to use whilst at the same time being quite computationally efficient; thus it was fairly easy for us to carry out large numbers of differently-parametrised serial **KMCLib** jobs on the **Eddie3** computing cluster here at Edinburgh. The codes used are kept here [18].

As we have MFT predictions about flow in a block, we can try to simulate that situation using KMC. In the bulk, the transition rates are simply those described in Figure 1. At the boundaries, referred to as the “top” and “bottom” of the block, there are 2 layers of lattice sites what switch between being full and empty with rates such that the time-averaged occupation can be specified to match the desired boundary conditions; there are then chances for particles to spawn and despawn with rates depending upon the occupation of these boundary layers. In the end, the intention is that these boundaries should reproduce the effect of having particle reservoirs attached

to the ends, which is something we can check for sanity in the output by inspecting the time-averaged occupations of sites near the boundary. I have used this setup to explore three scenarios, discussed in the following sections. In each of these I refer to a boundary condition configuration by  $(\rho_B, \rho_T)$ , with  $\rho_B$  and  $\rho_T$  being the bottom and top boundary densities respectively. When we measure flow rate in such a situation, we perform a specified number of Gillespie steps and count the number of particles entering at the top  $e_T$ , leaving at the top  $l_T$ , entering at the bottom  $e_B$ , leaving at the bottom  $l_B$ , as well as the Gillespie time interval  $T$  that elapses during those steps; we then have an estimate of the overall flow rate  $J$  via

$$J = \frac{e_B - e_T + l_T - l_B}{2T}. \quad (4)$$

We can also count the total number of particles in the system in order to measure the average particle density, although we need to make sure that it is correctly time-averaged; in my code this is done by updating a histogram of particle numbers as the simulation progresses. In each of our calculations, we make the initial configuration by randomly filling the system with particles and vacancies in such a way that the initial density should be  $\frac{1}{2}(\rho_T + \rho_B)$ , and then run the system for a specified number of equilibration steps to destroy any initial transients.

### A. Varying $\lambda$ with Fixed Boundary Conditions

The MFT we derived suggests that some kind of transition might occur as  $\lambda$  varies, as we go from a steady flow regime to a critically slow flow regime. An easy way to see if this happens is to hold the desired boundary densities constant whilst changing  $\lambda$ , and measuring the particle density as well as the mean, variance and skewness of the flow rate. If such a transition does indeed occur, we should expect to see a divergence in one of these moments. I have done this with 4 fairly exemplary sets of boundary conditions as shown in Figure 2. In each case we used systems of length 64 (length 32 gives similar results, so this is probably big enough), running them for 400000 Gillespie steps for equilibration followed by 10000 measurement runs of 1000 steps interspersed with relaxation runs of 16000 steps. This way we could gather statistics about flow rates and densities in a well-equilibrated system (if possible) whilst not having to worry too much about temporal autocorrelation effects.

### B. Varying $\lambda$ and Boundary Densities, Keeping the Average Density Constant

Another situation we can investigate has boundaries  $(\rho_B, \rho_T) = (\rho_M + \frac{1}{2}\delta\rho, \rho_M - \frac{1}{2}\delta\rho)$  for some given  $\rho_M$ , where  $\delta\rho$  and  $\lambda$  are varied. As before, I calculated flow rate moments and average densities, and the results are

displayed in Figure 3. These calculations were performed with the same run parameters (system length etc) as above.

### C. Diffusion Coefficient Measurement

Let us again specify the boundary densities to be  $(\rho_B, \rho_T) = (\rho_M + \frac{1}{2}\delta\rho, \rho_M - \frac{1}{2}\delta\rho)$  for some given  $\rho_M$ . This time we keep  $\delta\rho$  relatively small, so that  $J$  varies approximately linearly with  $\delta\rho$ ; thus if we calculate  $J$  for a series of small  $\delta\rho$ , we can perform linear regression to find  $D = \frac{\partial J}{\partial \delta\rho}|_{\delta\rho=0}$ , the effective diffusion coefficient. Computing this for different  $(\rho_M, \lambda)$  combinations gives us numerical data which can be compared with the MFT result in Equation 3. In this setup we ran the simulation for  $1.6 \times 10^8$  equilibration steps, followed by 10 sets of alternating measurement and relaxation runs, of lengths  $8 \times 10^7$  and  $1.6 \times 10^7$  steps respectively. We repeated the calculation with a system of half the size, and again found little difference between the two datasets, which gives us confidence that finite-size effects are small. We can of course obtain estimates of the confidence interval for our linear regression coefficient, and thus generate a standard error for  $D$ ; likewise we can obtain goodness of fit estimates for the regression. They are not included here for brevity, but they are in the additional materials.

### D. Flow Structure

It is possible to produce diagrams which show the changes in short-time-averaged local density as a function of space and time. I have made such diagrams for a selection of  $(\rho_M, \lambda)$  pairs, so that the reader can get an impression of what these flows actually look like; they are shown in Figure 5.

## IV. DISCUSSION

### A. Varying $\lambda$ with Fixed Boundary Conditions

Firstly, we should note that we only really have an MFT prediction for the flow rate as a function of  $\lambda$ . Technically we could attempt to predict the density as well, but we run into serious problems with solution uniqueness as soon as  $\lambda$  drops below  $\frac{1}{4}$ , which is when precisely things actually start to get interesting, so I haven't plotted it here. So long as we steer clear of regimes where the MFT predicts no flow, it is actually a decent enough predictor of the actual behaviour, becoming a better approximation as  $\lambda$  grows. However, one of the key predictions of the MFT, that a sharp transition to a no-flow regime occurs when  $\lambda$  becomes small enough (at least for 3 of the 4 sets of boundary conditions we investigated here), does not seem to be realised in our simulations. Indeed

what seems to be happening is that the sharp transition has been smoothed out, presumably by correlations the MFT does not consider; hence we do not see any peaks or jumps in the flow rate variance or skewness, which we would expect to see if there was a transition. As for the observed average density, for larger  $\lambda$  the density approaches the average of the boundary densities, and for small  $\lambda$  the density approaches 1 (which makes sense as the particles are very strongly attracted to each other, and so the system has a tendency to fill up); the exception to this is the case with extreme full/empty boundary conditions, although in this case one might argue that the particles are “sucked out” of the system so rapidly at the empty end that the system never really has a chance to fill up. It is also worth noticing that this extreme case is the only one in which the flow rate skewness does anything interesting; it is mostly positive, especially at low- $\lambda$ , implying that most of the time the system is fairly static, but occasionally short-lived strong flows occur which end up causing most of the bulk flow.

### B. Varying $\lambda$ and Boundary Densities, Keeping the Average Density Constant

The results gathered in the previous section are of course a special case of situation presented here; indeed, the graphs displayed in 3 Comparing the MFT prediction for the mean flow to what we observe in the numerics, we immediately see that, as before, the MFT is really quite effective at predicting flow so long as we avoid regimes in which flow is very small. Again, we don’t see spikes in the higher moments of the flow, indicating that hard transitions aren’t occurring. Finally, the density is very close to the average of the boundary densities until  $\lambda$  drops below  $\frac{1}{4}$ , which is consistent with our previous findings.

### C. Diffusion Coefficient

Putting the MFT prediction and the actual numerical results together as we have done in Figure 4, we can compare and contrast. The MFT seems to be a good predictor of the true behaviour of the diffusion coefficient, including the strange symmetry about  $\rho_M = \frac{2}{3}$  we pointed out in Section II B, so long as we avoid the region where the MFT predicts  $D < 0.4$ . The incorrectness of the MFT prediction suggests that some kind of nontrivial correlations have built up in this region, which makes sense as the coupling between particles has become stronger, whilst the density is middling, allowing that coupling to mean something. It is also worth noting that the discrepancy between intended density and actual density starts to become non-negligible here, which we can infer from how the originally rectangular grid of grey dots (indicating  $(\rho_M, \lambda)$  points where we obtained the data) has been deformed, to the extent that there is

a big cluster of them in the observed minimum of the diffusion coefficient. Some of these anomalous densities are greater than the density of the denser reservoir to which the system is coupled; thus, the reservoirs involved are in some sense “unphysical” as the data suggests that they would immediately attempt to switch to a higher density, which given a constant volume constraint would imply a phase separation occurs; thus the numerical results aren’t fitting so well into the paradigm we were using to analyse them (flow between reservoirs with slightly different densities), so it’s little wonder the MFT is having trouble keeping up. Of course, we do not see the negative diffusion coefficient that naive application of MFT would suggest, because it would cause instability; instead, the diffusion coefficient just becomes very small, as the system becomes unresponsive to concentration gradients.

### D. Flow Structure

Looking at Figure 5, we can make some observations. When  $\lambda$  is extremely low, the medium consists of solid blocks surrounded by empty spaces containing a dilute gas of particles; as we alter the overall density, all that changes is the thicknesses of these blocks. The case  $\lambda = 1$  is just excluded Brownian motion, and is included here for comparison. The most interesting images are those for the intermediate  $(\rho_M, \lambda)$ ; here we see a “lumpy” or “foamy” structure, in which small blocks of particles are being constantly created and destroyed whilst a rather minimal flow occurs across the system. We do not think that there is any hard phase transition as we vary  $(\rho_M, \lambda)$ ; rather, it seems that this “foamy” behaviour is part of a continuous range of phenomena between the extremes, containing medium-range correlations between particles. However, numerically computing equal-time correlation functions to the accuracy required to draw conclusions about these correlations has proven to be extremely difficult, so we cannot speak in quantitative terms about them.

### E. Conclusions

To conclude, the continuum MFT is a surprisingly good predictor of the bulk flow behaviour of the SPM, provided we avoid the region where it breaks down. That, combined with interpolations of our data about the flows during breakdown, could form the basis of a large-scale approximation of the flow, which could be used to make a PDE model of, say, interface growth on metal surfaces. Further study is required, of course; in particular it would be interesting to generalise this model to multiple species inhabiting coupled lattices, as this could inform us about the oxidation of alloys, such as niobium-enriched titanium.

- 
- [1] V. Belitsky and G. M. Schtz, Journal of Statistical Mechanics: Theory and Experiment **2011**, P07007 (2011).
- [2] M. Mobilia, I. T. Georgiev, and U. C. Täuber, Journal of Statistical Physics **128**, 447 (2007).
- [3] B. Tegner, L. Zhu, C. Siemers, K. Saksl, and G. Ackland, Journal of Alloys and Compounds **643**, 100 (2015).
- [4] L. Zhu, Q.-M. Hu, R. Yang, and G. J. Ackland, The Journal of Physical Chemistry C **116**, 24201 (2012).
- [5] B. E. Deal and A. Grove, Journal of Applied Physics **36**, 3770 (1965).
- [6] N. Cabrera and N. Mott, Reports on progress in physics **12**, 163 (1949).
- [7] A. J. Ladd, M. E. Colvin, and D. Frenkel, Physical review letters **60**, 975 (1988).
- [8] T. M. Liggett, *Interacting particle systems* (Springer-Verlag, Berlin, 1985).
- [9] M. Kardar, G. Parisi, and Y.-C. Zhang, Phys. Rev. Lett. **56**, 889 (1986).
- [10] J. Krug and H. Spohn, Phys. Rev. A **38**, 4271 (1988).
- [11] K. Sugden and M. Evans, Journal of Statistical Mechanics: Theory and Experiment **2007**, P11013 (2007).
- [12] S. Katz, J. L. Lebowitz, and H. Spohn, Journal of Statistical Physics **34**, 497 (1984).
- [13] R. K. P. Zia, Journal of Statistical Physics **138**, 20 (2010).
- [14] K. Kawasaki, Phys. Rev. **145**, 224 (1966).
- [15] M. R. Evans and B. Waclaw, Journal of Physics A: Mathematical and Theoretical **47**, 095001 (2014).
- [16] B. Waclaw and M. R. Evans, Physical review letters **108**, 070601 (2012).
- [17] M. Leetmaa and N. V. Skorodumova, Computer Physics Communications **185**, 2340 (2014).
- [18] J. Hellier, “Codes for Sticky Particles in 1D,” (2017).

FIG. 2. Moments of flow rates and average overall densities observed when varying  $\lambda$  with fixed boundary densities  $(\rho_B, \rho_T)$ : Blue refers to  $(\frac{2}{3}, \frac{2}{3})$ , yellow to  $(\frac{3}{4}, \frac{7}{12})$  (both with average density  $\frac{2}{3}$ ); green to  $(\frac{3}{4}, \frac{1}{4})$ , red to  $(\frac{99}{100}, \frac{1}{100})$  (with average density  $\frac{1}{2}$ ). In the case of the mean flow we have an MFT prediction, indicated by the solid line.

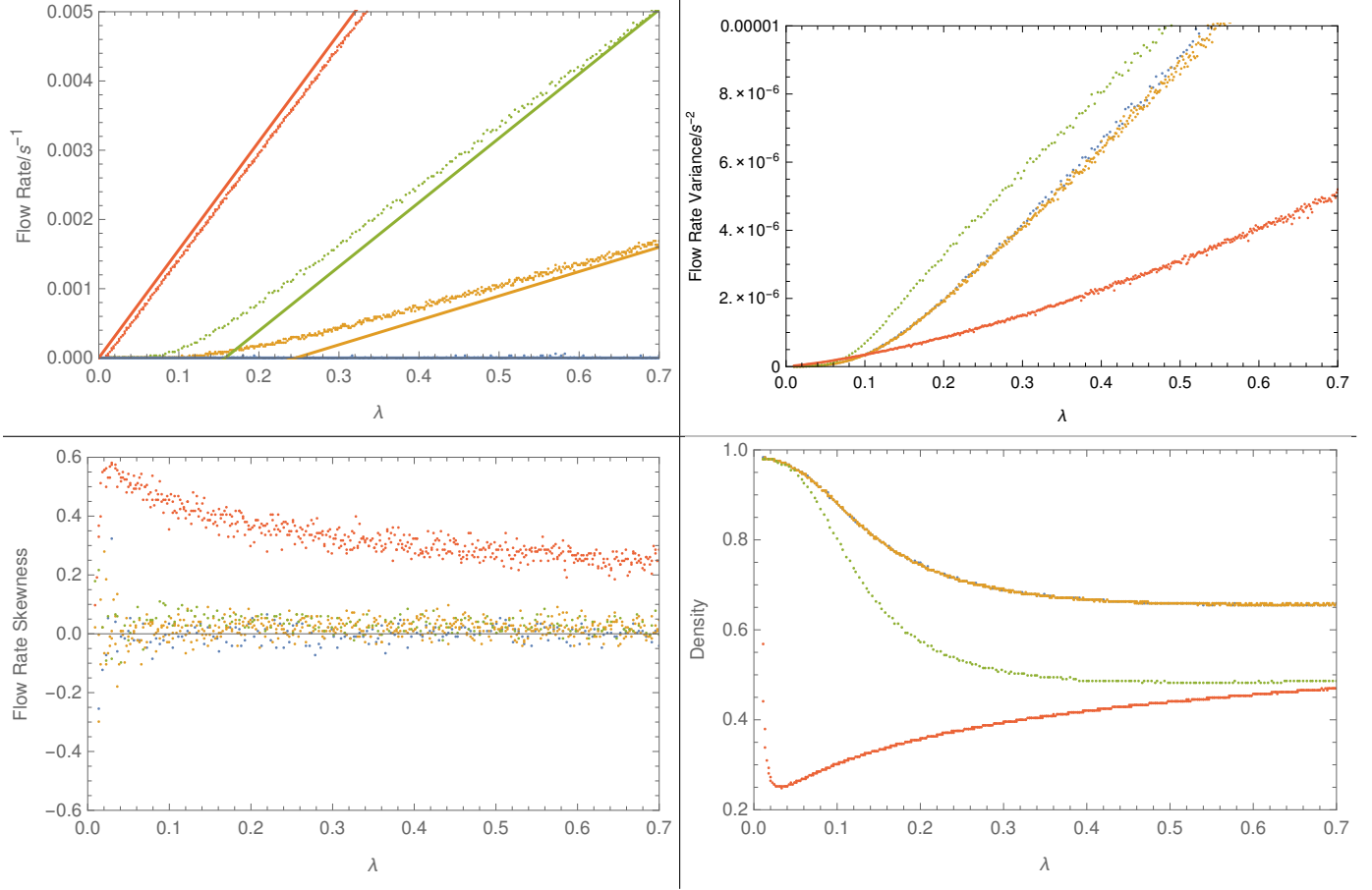


FIG. 3. Flow rate mean, flow variance and average overall densities observed when varying the difference  $\delta\rho$  between the boundary concentrations  $(\rho_B, \rho_T) = (\rho_M + \frac{1}{2}\delta\rho, \rho_M - \frac{1}{2}\delta\rho)$  and  $\lambda$ . I chose  $\rho_M = \frac{1}{2}$ , as this gives us the biggest range of  $\delta\rho$  to investigate. The top left panel is the MFT prediction for the flow rate, whilst top right shows the observed mean flow rate. The measured flow skewness and kurtosis are not displayed here as both signals were small and noisy, and didn't show anything particularly significant.

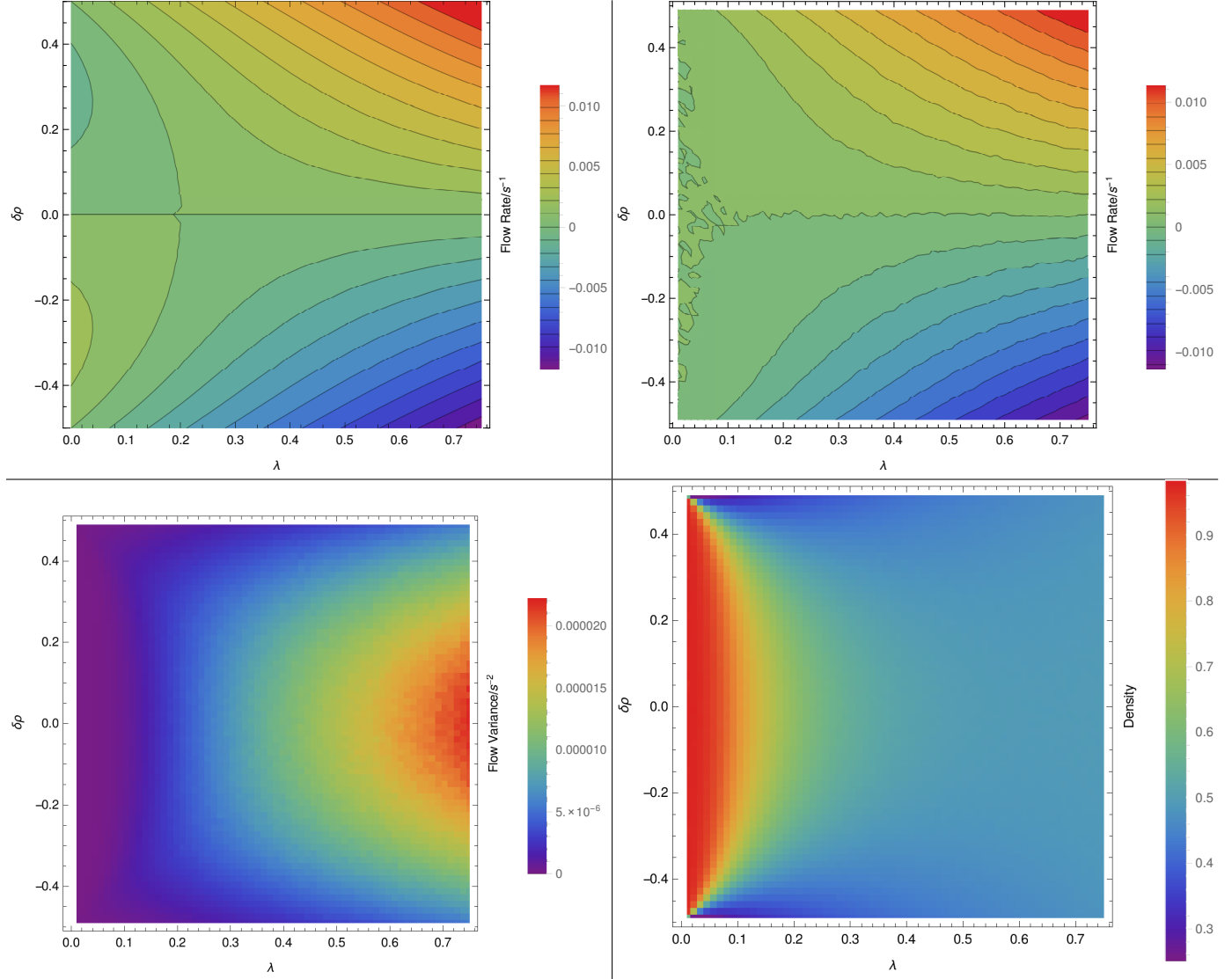


FIG. 4. The contour plot on the left shows the MFT prediction of the diffusion coefficient  $D = \frac{\partial J}{\partial \delta \rho} \Big|_{\delta \rho=0}$  as a function of local density  $\rho_M$  and  $\lambda$ ; we are only plotting where  $0 \leq D \leq 1.2$ , other regions are shown in white, including the region in which  $D < 0$ , which would cause instabilities and so prevent a flow from actually occurring. On the right is our numerical calculation of  $D(\rho_M, \lambda)$ , with exactly the same plotting ranges. The dots indicate which points in  $(\rho_M, \lambda)$  we calculated  $D$  around, to give an impression of how the interpolation in the contour plot was done.

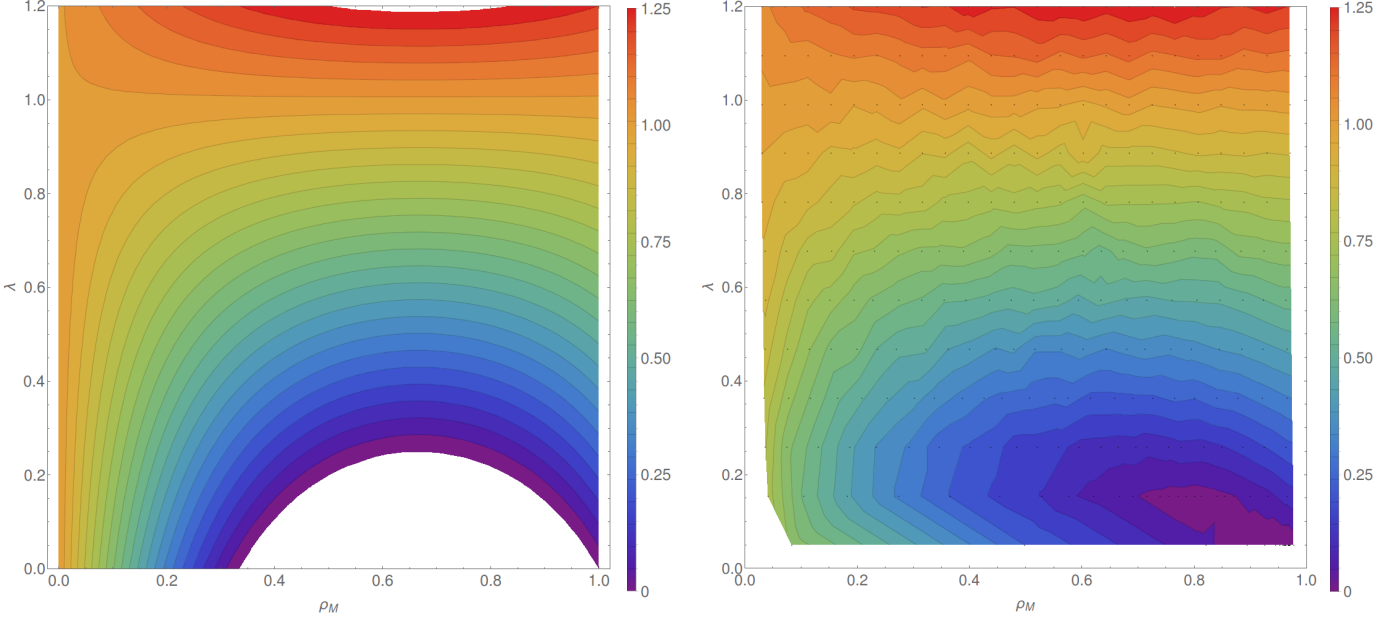


FIG. 5. The spacetime flow patterns, for the  $(\lambda, \rho_M)$  combinations indicated in the row and column headers. In each plot time runs along the  $x$ -axis, space along the  $y$ -axis. White represents full occupation, black empty, and grey shades partial occupation. The degree of occupation was calculated by taking the `KMCLib` record of a particular site's occupation (i.e. the Gillespie times at which the site changed occupation), assigning 0 and 1 to particles and vacancies respectively, linearly interpolating this and then integrating over times longer than a single Gillespie step but much shorter than the total time in question. In each case the total time elapsed is that taken by  $10^6$  Gillespie steps, and each short-time-average has been done over the total time divided by 508 (to produce square diagrams, as there are 508 active sites per simulation). Time has been rescaled this way in order to allow fair comparison of radically different  $\lambda$ -values.

